

Comparison of calibration methods for the reconstruction of space-time rainfall fields in Southern Italy

Arianna Orasi^{a*}, Giovanna Jona Lasinio^{b*}, Clarissa Ferrari^{b*}

31st March 2005

Abstract

The role of rainfall raingauge observations in calibration of radar derived rainfall estimates is investigated. The final goal is the reconstruction of the rainfall fields over the observed area. As a first step, an operational approach commonly used by hydrologists is applied and results are discussed. In the sequel a space-time approach based on the work of Brown et al. (2001) and the use of kriging with external drift are applied and compared. Data come from a dense raingauge network and a weather radar installed in 1992 for the evaluation of a rain enhancement experiment carried out in Southern Italy. In this paper we report results from one seeding operation carried out on 11 April 1992.

Keywords: radar, rainfall, space-time, kriging, external drift, dynamic linear model, Kalman filter, weather modification.

^{a)}University of Bologna, Bologna, Italy, orasi@stat.unibo.it, ^{b)}DSPSA, University of Rome "La Sapienza", Rome, Italy, giovanna.jonalasinio@uniroma1.it

1 Introduction

The Rain Project was an Italian randomized rain enhancement plan applying in Puglia and other regions of Southern Italy, methods and technology of rain enhancement used in the Israeli experiment (Gagin (1981)) were tested. The project was developed in the period 1986-1994 during which cloud seeding operations were carried out over two experimental, Target and Control, areas. The selection of these experimental two areas depended entirely on the statistical analysis of available climatology of the region with special emphasis given to the pluviometric database and its natural variability. Seeding paths were selected according to the effective upper wind direction measured in-flight by pilots. Silver Iodide (AgI) in acetone solution was used as reagent. In 1992, important implementations to the project were introduced. In particular, a high density network of 80 automated raingauges with high time (10 minutes) and space (~ 10 km inter-gauge spacing) resolution was built in the experimental area. Moreover, in the same year, a C-band digital weather radar, scanning the whole area every five minutes, with software to analyse the effects of seeding on the vertical structure and on the humidity content of the seeded clouds was introduced. The seeding campaigns were carried out in different seasons starting from April 1992 until May 1994, when the project was stopped. The total number of missions was 132, but operational inconveniences (e.g. radio noise, unclear radar images, chaotic distribution of echoes, radar failure, unavailable wind reports) reduced the total number of reliable cases to 116.

The development of several approaches to assess results of seeding, based on experimental rain gauge data and physical evidence, was carried out during this period without obtaining a clear and definitive answer. One reason for this result is that expected effects of seeding are almost always within the range of natural variability (low signal-to-noise ratio) and skill in predicting natural behavior is still limited. Comparison of precipitation observed during seeded periods with that during historical periods presents problems due to climatic and other changes in time and therefore is not a reliable technique. This situation has been made even more difficult by the mounting evidence that climate change may lead to changes in global precipitation amounts as well as to spatial redistribution of precipitation.

In currently accepted ways of evaluation, randomization methods (target/control, crossover or single area) are considered the most reliable for detecting cloud-seeding effects. Such randomized tests require a number of cases readily calculated on the basis of natural variability of the precipitation and the magnitude of the expected effect. In the case of very low signal-to-noise ratios, as in the present case, experiment duration in the range of five to over ten years may be required (W.M.O. (2001)). All these reasons raised the need to find alternative ways to those evaluation procedures previously applied in the Italian Rain Project.

Our idea is to reconstruct the rainfall field (in both space and time), using both radar and rainfall observations, and use the results to compare Target and Control area estimated rain amount for each seeding operation in order to assess the efficacy of the experiment.

In this setting, the major benefit in using radar data is the finer spatial description of the precipitation field that this instrument produces, on the other hand a major disadvantage is the need to calibrate radar parameters used for converting reflectivity values to rain; this generally requires the installation of a conventional ground-based rain gauge network. Raingauges' observations are considered close to the true rainfall and this is why raingauges estimates of rainfall are used to calibrate radar-based rainfall quantities.

The investigation of the role of raingauges observations in the calibration of radar derived rainfall estimates for the reconstruction of the rainfall fields becomes a central issue.

In the following sections the technique of calibrating weather radar using data from rain-gauges is illustrated. In particular, in section 4 an approach to the calibration process using an operational technique (Collinge and Young (1993)) is described. This technique involves the computation of a *calibration factor* used to adjust rainfall rates produced by the well-known Marshall-Palmer relationship. In section 5 a space-time approach is proposed. The model, inspired by the work of Brown et al. (2001), is built as a combination of unidimensional state-space time series and time-varying kriging surfaces of the dynamic regression model coefficients. The predictive performance of the model is investigated through empirical validation. Moreover, a spatial method known as Kriging with external drift, is applied considering rain-gauges' data as a random function and the radar data, as the external drift function. Again, the predictive performance of the model is investigated through empirical validation. As a further term of comparison, simple Ordinary Kriging of the precipitation measurements are computed and the empirical MSE at validation sites of the three models are compared and discussed. Results are reported in section 6.

It is important to stress that the aim of this paper is to investigate the relationship between rainfall at rain-gauges and radar reflectance. Several statistical models exist for modelling precipitation, a task we do not intend to undertake. However we refer the interested reader to the extensive literature available on this topic; here we report only a brief outline of papers which have been of inspiration for our work. Dunn (2003) made one of the earliest attempts introducing a family of distributions that can model the amount of precipitation including those observations in which zero rainfall is recorded. The works of Sansó and Guenni (2000) and Sansó and Guenni (1999) consider a model for daily rainfall based on a truncated normal distribution in a Bayesian framework. In Rodriguez-Iturbe et al. (1987) and Rodriguez-Iturbe et al. (1988) stochastic point processes based models in space and time are used. A different approach is considered in Smith (1994) where, as in Stern and Coe (1984), they distinguish between processes for wet and dry periods and they introduce a positive skewed distribution for the amount of rainfall, conditionally on a wet period.

2 Rainfall measurements: wheatear radar and raingauges

Radar serves the estimation of rainfall, either on its own or, more often, in combination with rain-gauges. Radar data, although sometimes erroneous in magnitude, have the great advantage that they provide a coherent image of spatial rainfall patterns, which, especially in case of small-scale convective events and/or coarse rain gauge networks might miss altogether.

A wheatear radar can provide measurements of precipitation intensity over a wide area with high spatial and temporal resolution, from a single location. But rainfall and radar measurements can be notably different: on one hand the first give a direct measurement, spatially punctual and time integrated, of ground rainfall; on the other, the second ones provide indirect measurements of precipitation, on the air, and integrated in space and at a given point in time. To mitigate the sometimes large discrepancies of radar to rain gauge observations numerous techniques have been developed that try to approach radar to rain gauge measurements. In order to allow a comparison between the two, rain measurements are integrated for a period of time so that a temporal integration corresponds to a spatial one made by radar (Zawadzki (1975)).

In a meteorological radar, a pulse of energy is emitted by the transmitter at a variety of elevation angles and the returned power, or *reflectivity*, is measured at a radial resolution of 1 km. Data are expressed in radar reflectivity units of dBZ. This is a measure of the power scattered back to the radar by precipitation particles in the atmosphere. Meteorologists commonly convert from reflectivity (Z) to a rainfall rate (R) using the Marshall-Palmer law (Marshall and Palmer (1948)). Unfortunately, the relationship between Z and the rainfall rate R (in mmh^{-1}) is not exact. Most of the conversions, called Z-R relationships, result in the following power law expression:

$$Z = aR^b \quad (1)$$

where a and b are unknown coefficients. Available estimates of a range from about 30 to 500 and b range from about 1.2 to 2.0 (Doviak and Zrnica (1984)).

Relationship of this type should be regarded as empirical, although a strong theoretical justification exists for this choice. Actually, both radar reflectivity and rainfall rate can be expressed as the moment of the drop size distribution within a radar sampling volume. This is where the first problem appears when using raingauge observations for parameter estimation in the Z-R relationship. Most raingauges do not measure rainfall rate but rather, rainfall accumulation. This problem, when combined with the extremely high space and time variability of the rainfall process, indicates that no high correlation between raingauge observed rainfall and radar-estimated rainfall at short time scales (Krajewski (1997)) should be found. Moreover several factors can affect the precision of radar measurements of rain rate and the actual rain rate at ground level. Errors could be random, systematic and/or dependent on the distance from the radar (Zawadzki (1984)). In particular, as the distance from the radar increases, radar measurement quality can worsen, because of:

- 1) the presence of a precipitation gradient inside the cell (which becomes larger due to the divergence of radar beam);
- 2) the attenuation of the radar signal;
- 3) the radar signal for low elevations and high distances could be behind the cloud's base;
- 4) the variability of the Drop Size Distribution (DSD) at ground level within each storm and from storm to storm;
- 5) the minimum detectable signal at far distances.

For these reasons radar measures have to be corrected.

A huge amount of studies covers the issue of comparing radar and raingauge, as Austin (1987), Ciach and Krajewski (1999), Legates (2000), Matsoukas et al. (1999) and Wood et al. (2000).

Co-kriging and other geostatistical methods (Krajewski (1987)), (Seo et al. (1990)), (Seo et al. (1990)) are widely used methods to adjust the Z-R-relation to match rain-gauge observations. However, even sophisticated methods merging rainfall observations from different devices are limited by the quality of the input data.

Our input dataset is composed of rainfall and reflectivity measurements, collected every ten minutes and coming, respectively, from the CPP¹ network and the weather radar from 1992 to 1994. Data validation is critical as severe errors in data analysis and modelling results can be caused by erroneous individual data values. In addition, before performing any analysis, considerable attention was devoted to data quality control, for details see Orasi and Jona-Lasinio

¹Raingauges network installed in 1992 for the evaluation of the Rain Project. CPP stays for *Controllo Progetto Pioggia*

Apr. 1992	Oct. 1992	Nov. 1992	Dec. 1992	Feb. 1993	Mar. 1993
44	55	57	57	57	62
Apr. 1993	Jan. 1994	Feb. 1994	Mar. 1994	Apr. 1994	May 1994
58	65	62	42	59	58

Tab 2.1: Total number of reliable stations for the 12 months of seeding operations

(2004) and Orasi (2004).

The quality control analysis of the raingauge network has shown that the network did not always performed well. Most of the problems were due to blockages of a large numbers of gauges. The number of reliable stations ranges from a minimum of 42 to a maximum of 65 (see Table 2.1).

The radar reflectance values at a gauge site is assumed to be the value at the nearest radar pixel center. Anomalies and occasional spikes were removed from reflectance values by a median smoothing procedure.

3 The core dataset

In the following Sections 4, 5, 6 and 7 attention is focused on rain data collected, every 10 minutes, on April 11, 1992 by the weather radar station located in the Airport of Bari Palese and by 44 out of the 80 raingauges belonging to the CPP network, already considered as reliable raingauges. Our choice is motivated by the fact that, the most complete set of data, regarding both ground and radar measurements belongs to this day. Figure 1 shows the 43 raingauges involved in the analysis and the six gauges reserved for validation are indicated in blue.

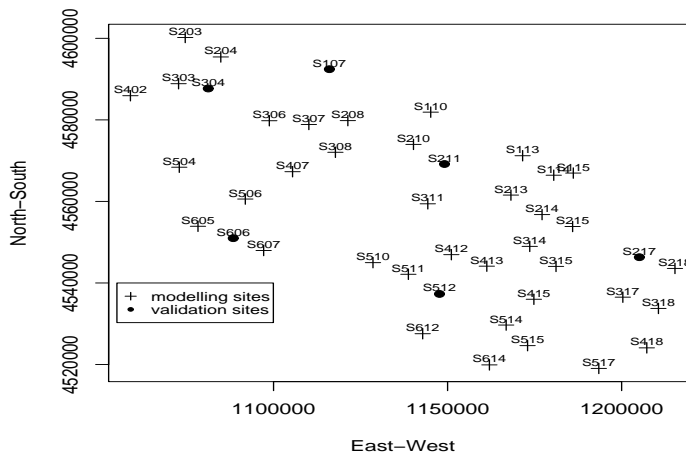


Figure 1: Base map of raingauges

The rainfall event starts at 5:10a.m. and ends at 10:00a.m of the same day. The length of the time series is $T=30$. A geographical selection of radar-rainfall data was performed in order to remove data at the edge which are less accurate. Starting grid nodes were 15600 and performing a geographical selection, the output grid counts 2754 nodes. Reflectance values are

then available on a grid of $N=2754$ pixels, each 2 km square. In the sequel we use 38 out of the 43 reliable stations for modelling purposes and 6 raingauges for validation.

3.1 Some exploratory data analysis

In Figure 2 the mean rainfall at each of the 38 modelling sites is reported. This shows the dry aspect of the considered region.

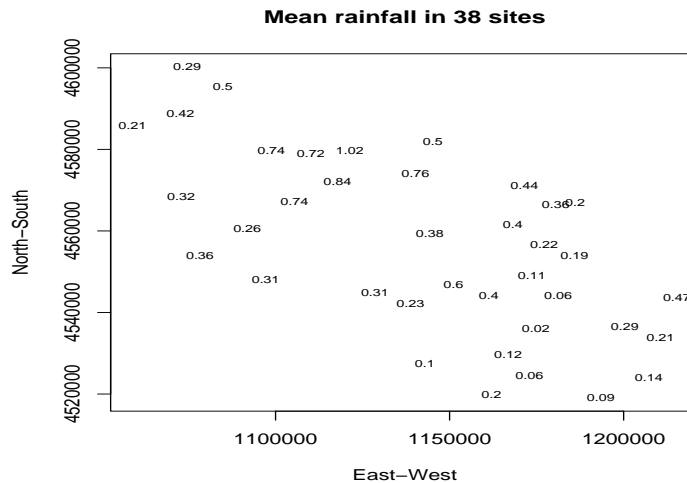


Figure 2: Mean rainfall for 38 modelling sites (6 raingauges are used for validation purpose)

In Figure 3 we report the average rain at each modelling site corresponding to a log radar value; it is easily seen that a linear relationship exists between the two measures on the log scale.

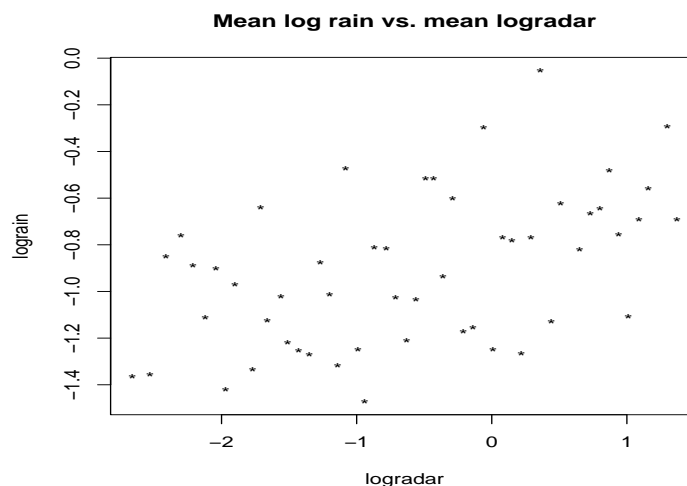


Figure 3: Mean of log rainfall vs log radar for the 38 modelling sites

The spatial variation of rainfall is investigated by using an empirical variogram of the data computed following Sahu and Mardia (2005). We first obtain the residuals after fitting a regres-

sion line using logradar at each site as covariate. We also remove any temporal variation and trend present in the residuals by explicit modelling or by creating successive differences. Let $W(\mathbf{s}_i, t)$ denote the residuals. We suppose that $W(\mathbf{s}_i, t), t = 1, \dots, T$ are independent replications at location $\mathbf{s}_i, i = 1, \dots, n$ since we have de-trended the data. We now consider the average variogram defined by

$$\gamma(d_{ij}) = \frac{1}{2T} \sum_{t=1}^T E[\{W(\mathbf{s}_i, t) - W(\mathbf{s}_j, t)\}^2]$$

where d_{ij} is the distance between the spatial locations \mathbf{s}_i and \mathbf{s}_j . The quantity $\gamma(d_{ij})$ is estimated by

$$\hat{\gamma}(d_{ij}) = \frac{1}{2T} \sum_{t=1}^T \{w(\mathbf{s}_i, t) - w(\mathbf{s}_j, t)\}^2.$$

The empirical variogram cloud is obtained by plotting $\hat{\gamma}(d_{ij})$ against d_{ij} for the $n(n-1)/2$ possible pairs of locations.

In Figure 4 we provide the variogram cloud and we super-impose a smooth loess curve (as obtained using the R function `loess`). The spatial structure is quite regular allowing us to accept the use of classical geostatistical tools to estimate rainfall values.

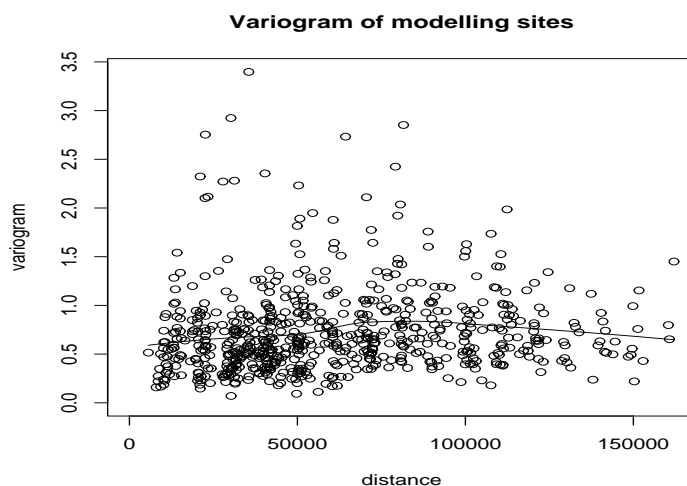


Figure 4: Empirical variogram for the 38 modelling sites

The temporal structure of spatial mean rainfall values is investigated (Figure 5) through the autocorrelation function that decreases within one hour time window. In Figure 6 the same plot is reported for radar rainfall estimates. It clearly shows that a calibration must be carried on. The temporal structure is almost the same in terms of autocorrelation. However a direct conversion of radar values based on standard techniques (see next paragraph) is unsatisfactory.

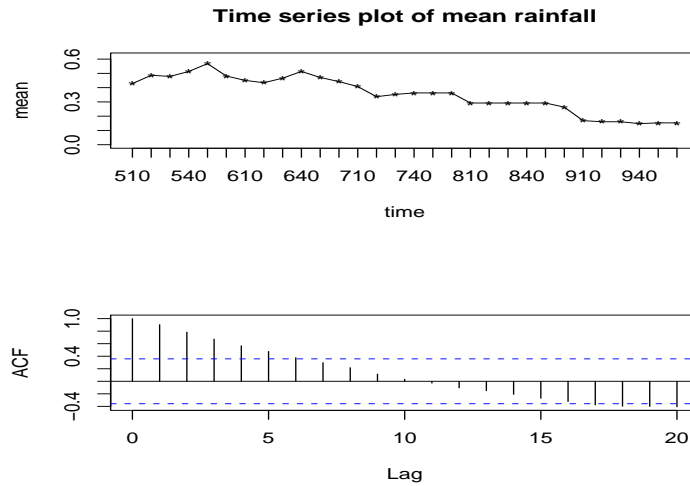


Figure 5: Time series plot and autocorrelation function of spatial mean rainfall for 38 modelling sites

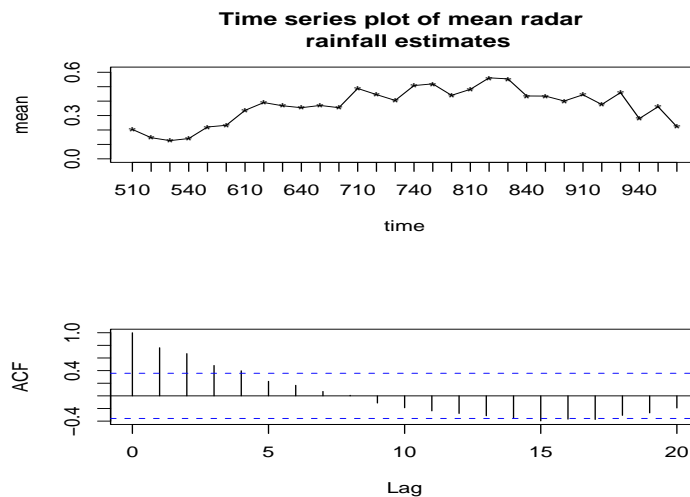


Figure 6: Time series and autocorrelation function of spatial mean radar rainfall estimates for 38 modelling sites

One station out of the 44 reliable raingauges had to be removed. This station (S415-Pizziferro Argento) showed radar-based rainfall estimates reporting all zero values and had to be considered as an outlier. Then rainfall values at this raingauge and the corresponding radar-based rainfall estimation at the same location were discarded from the subsequent analysis. In the next section we will investigate in detail the direct conversion of radar measurements into rainfall and an operational technique for the radar calibration.

4 An operational technique: the calibration factor

Data from a calibrating rain gauge with the corresponding radar observations provide the *calibration factor*:

$$CF = \frac{\text{gauge} - \text{rainfall}}{\text{radar} - \text{rainfall}} = \frac{R_g}{R_r} \quad (2)$$

This factor is used to adjust rainfall rates produced by the conversion equation (1); the method is equivalent to choose a new value for a . The *bias*, if n is the number of the calibration gauges, is:

$$CFq = \frac{\sum_{i=1}^n (R_g)_i}{\sum_{i=1}^n (R_r)_i} \quad (3)$$

Equation (3) associates a weight proportional to its value to each observation. It is expected that the *calibration factor* could vary spatially in a systematic way. Therefore, we aim to describe the spatial variability of the calibration factor and of the *bias* in order to perform spatial adjustment choosing different *bias* calibration factors or the averaged *bias* calibration factor computed according to the distance from the radar. There is usually an increase in the calibration factor with distance from the radar. Actually, it is expected that the accuracy of the radar measurements decrease with increasing distance from the radar site so that adjustment at any point can be made by referring to the nearest calibration gauges rather than using an average calibration factor over the whole area. The radar-based rainfall estimation was obtained using the Z-R relation (1) with $a = 200$ and $b = 1.6$ (Marshall and Palmer (1948)).

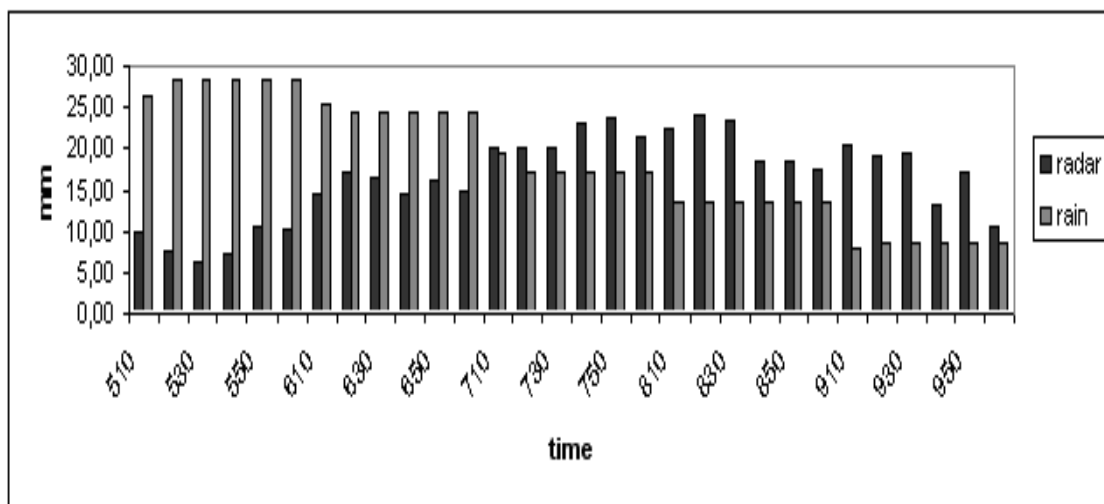


Figure 7: Total precipitation measured by the reliable raingauges (*dark bar*) starting from 5:10 a.m. until 10:00 a.m. on April 11, 1992 compared to the total of the estimated radar-rain (*light bar*) for the same period

Figure 7, for instance, shows the sums of the rain collected by the reliable ground raingauges each 10-minutes on the April 11, 1992 from 5:10 a.m. until 10:00 a.m. and of the radar-based rainfall estimation for the same period. The maximum amount of rain is achieved in the interval 5:20 a.m.-6:00 a.m while the maximum amount of radar-based rainfall estimations is achieved at 8:20 a.m. Starting from 8:20 a.m., the amount of rain decreases in both cases even if the radar-based estimations are always larger than the observed rain.

A general comment for all analysed periods is that the complexity of the radar instrumentation and measurement procedure, as well as the complexity and enormous variability of the rainfall process, suggest discrepancies in radar-rainfall and raingauge rainfall products. The sources of these discrepancies may be as simple as electronic miscalibration of the radar instrument, or a non exact Z-R relationship.

In order to calculate the *calibration factor*, the ratios between the rain collected by each raingauge, cumulated during the considered period, and the radar-based rainfall estimations cumulated for the same period, are computed and plotted against the distance of raingauges from the site where the radar is installed. This procedure was applied to all events considered reliable and findings show that, although ratios values should be near to one, generally, it is not often the case regardless of the distance from the radar. Figure 4 reports, as an example, *calibration factor* values of April 11, 1992 against distance from the radar.

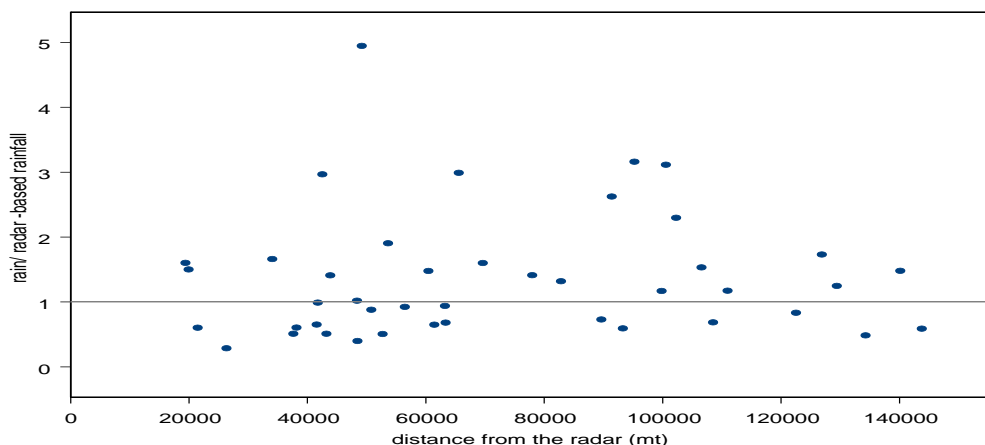


Figure 8: Ratio values against distance from the radar located at Bari Palese Airport, April 11, 1992

Furthermore, in general, results show that the distance of raingauges from the radar does not influence ratio values. A single *bias* calibration factor is enough to cover the entire study area. According to these results an adjustment of radar-based rainfall estimations was proposed using the overall mean of the calibration factors, without introducing the variable "distance". The required *calibration factor* was obtained for each event considered separately.

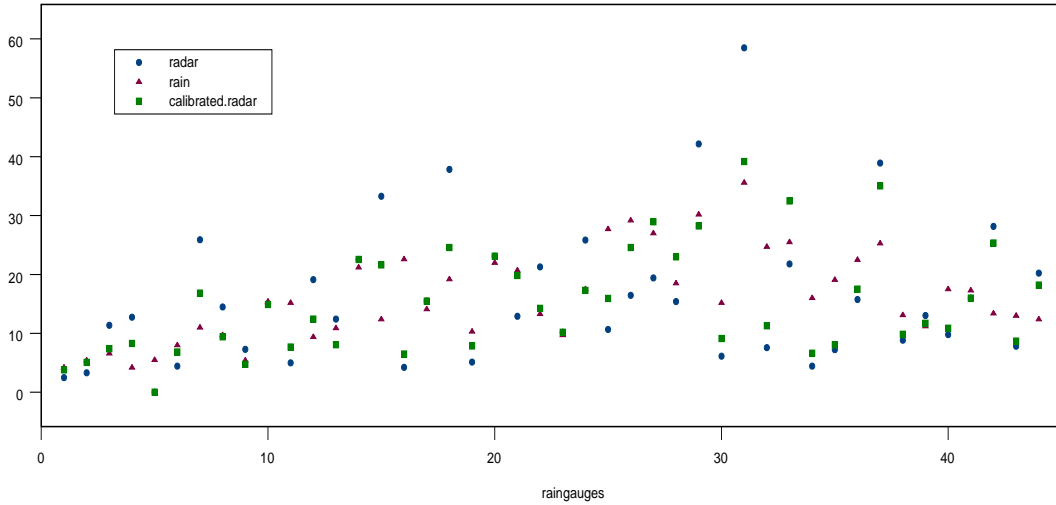


Figure 9: Rain, radar estimates and radar calibrated, at each reliable raingauge, for the 11 April 1992

For instance, in Figure 9, at each raingauge, radar-based rainfall estimations corrected by the single *bias* calibration factor, the raw radar measurements and the gauge rainfall cumulated during the 11 April 1992 are plotted. Results show that there is a reduction in the errors in radar estimates even though spatial errors still remain. This fact allows us to state that as the time integration increases, some of the typical problems as zero-rainfall intermittence, small-scale rainfall variability and raingauge measurement error become less pronounced.

As concluding remarks notice that there are several major drawbacks in this operational calibration technique:

- the *calibration factor* becomes infinite when the radar reading $R_r = 0$ and the raingauge value $R_g > 0$ and viceversa for the *assessment factor*.
- the simple averaging does not allow for the variation in time of the two factors, that is the estimator has no "dynamic" memory.
- there is no natural way to compute the *calibration factor* where raingauges are not available.

5 A space-time approach

To exploit the intense spatial coverage offered by the radar and the temporal density of the raingauges data, following Brown et al. (2001), a time-series model is fitted at each site, using a linear Gaussian state-space regression starting from the relationship between raingauges data and radar reflectance values (Collinge and Young (1993)):

$$R_{gt} = aR_{rt}^b * e_t \quad (4)$$

where R_{gt} is the gauge measurement at time t , R_{rt} is the radar measurement, e_t is a multiplicative error term and t indicates the sampling time. An exploratory spatial analysis is conducted

over the outputs of the n single-site models.

5.1 Single-site modelling

In this part we consider each site separately when both raingauges' data and radar-rainfall estimates are recorded at regular time-intervals during a rainfall event. The basic hypothesis is that the relationship between the two measurements is assumed to be given by equation (4) (Collinge and Young (1993)). In order to rely on a linear Gaussian state space model the logarithms are taken as follows. Let I_t be a binary process assuming values 1 if $R_{gt} > 0$ and 0 otherwise. In this case the observed process \tilde{R}_{gt} can be modelled as the product of two processes $\tilde{R}_{gt} = I_t \times R_{gt}$, then we log-transform only the R_{gt} part of the process and we model it according to the following scheme.

Parameters a and b in Eq.(4) are assumed to be varying over time and can be represented as first order autoregressive models. Therefore the *observation equation* and the *state equations*, conditionally on $I_t = 1$, are:

$$\begin{aligned} y_t &= \alpha_t + W_t \beta_t + \epsilon_t \text{ for } t = 1, \dots, T. \\ \alpha_t - \mu_\alpha &= \phi_\alpha (\alpha_{t-1} - \mu_\alpha) + \eta_t \\ \beta_t - \mu_\beta &= \phi_\beta (\beta_{t-1} - \mu_\beta) + \varepsilon_t \end{aligned} \quad (5)$$

with $y_t = \log(R_{gt})$, $W_t = \log(R_{rt})$ and the time-series ϵ_t , η_t , ε_t zero-mean, white-noise sequence with variances σ_ϵ^2 , σ_α^2 , σ_β^2 respectively. Parameters ϕ_α and ϕ_β are autoregressive parameters and are estimated together with the remaining unknown parameters, namely, σ_ϵ^2 , σ_α^2 , σ_β^2 , μ_α and μ_β , by maximum likelihood (MLE). The Kalman filter² produces both the minimum squared error estimates of the regression coefficients α_t and β_t and the likelihood function for the model (5).

5.2 Estimation of single-site models

Results obtained at site 210 are reported as an example. This site has recorded high rainfall values compared to the other raingauges during the analyzed period, furthermore it does not contain zero values. Figure 10 shows data on the log scale. In Tab. 5.2 values of the MLE parameters estimation are reported.

²The output of Kalman filter was estimated by SsfPack package of Ox language

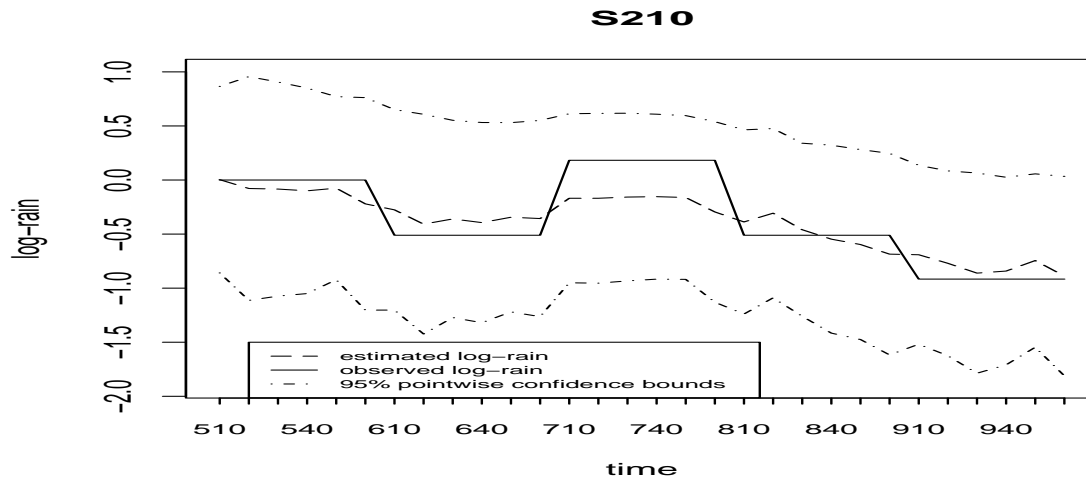


Figure 10: Radar-rainfall estimates, raingauges' data and 95% pointwise confidence bounds at site 210

Parameters	MLE
σ_{ϵ}^2	0.123
σ_{α}^2	0.0116
σ_{β}^2	0.00348
μ_{α}	-0.00206
μ_{β}	0.00003
ϕ_{α}	1.0
ϕ_{β}	0.99783

Tab 5.1: MLE estimates of parameters in model (5) at site 210

In Figure 11 the minimum mean square error predictors of the state α_t and β_t provided by the Kalman filter are drawn against time with their empirical pointwise 95% confidence bound.

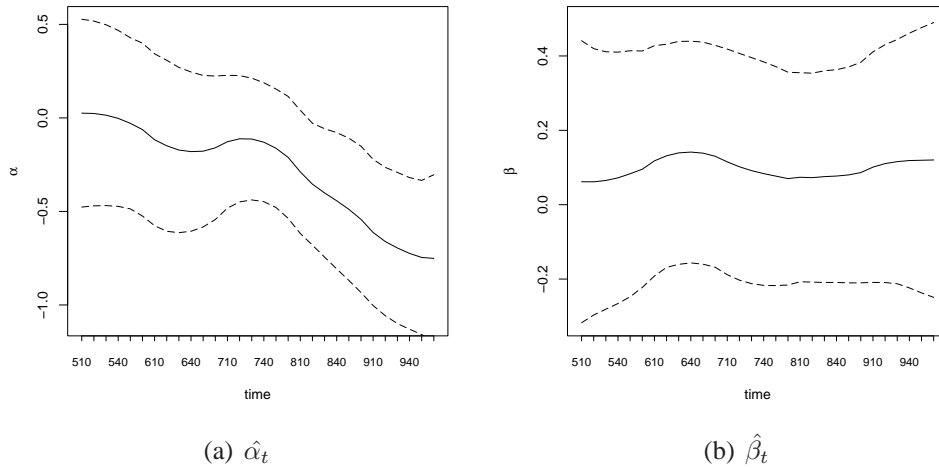


Figure 11: Prediction of states α_t and β_t at site 210

The most evident feature of the figure is that $\hat{\alpha}_t$ decreases when $\hat{\beta}_t$ is constant or increases. This fact is common to all sites.

Furthermore we investigate the behavior of $(\hat{\alpha}_{it}, \hat{\beta}_{it})$ for $i = 1, \dots, n$ and $t = 1, \dots, T$ which are the minimum mean square error predictors of the dynamic regression coefficients, obtained from the single-site models fitted to data from each of the n sites. Computation of the sample autocovariances of the arrays $\hat{\alpha}_{it}$ and $\hat{\beta}_{it}$ point out an exponential decay with increasing time-lag, then the assumption of a first-order autoregressive model is consistent. As an example, the partial autocorrelation functions of $\hat{\alpha}_t$ and $\hat{\beta}_t$ at site 210 are reported in Figure 12.

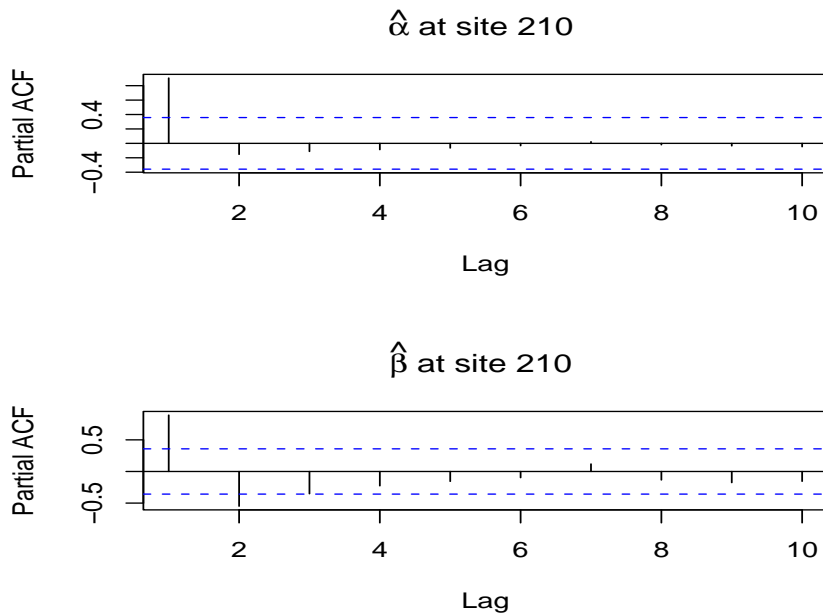


Figure 12: Partial acf of $\hat{\alpha}_t$ and $\hat{\beta}_t$ at site 210

5.3 The integrated model

Our aim is to combine the results from the previous section into an integrated model to describe the relationship between radar-rainfall based estimates and raingauges' measurements on the $2km \times 2km$ pixel grid. Radar data are available at each of the $N = 2754$ pixels of the grid while raingauges' values are recorded at 43 sites. The model is defined on the set of N pixels and the measurements y_{it} at non-gauge sites are considered as missing. The unobserved values of y_{it} are predicted as:

$$\hat{y}_{it} = \hat{\alpha}_{it} + \hat{\beta}_{it}W_{it}. \quad (6)$$

Therefore, the predictions of $\hat{\alpha}_{it}$ and $\hat{\beta}_{it}$ at non-gauge sites have to be constructed.

Recall that in this procedure the modelling sites are $n = 38$ (of which one had to be removed because all radar measurements were zero) and 6 sites are set a part for validation. We choose to consider the outputs of the n single calibration sites $(\hat{\alpha}_{it}, \hat{\beta}_{it})$ for $i = 1, \dots, n$ and to perform the estimation over the whole area covered by the radar, conditionally on each temporal slice, through an ordinary kriging (OK). This method allow us to obtain time-varying kriging surface of both $\hat{\alpha}_{it}$ and $\hat{\beta}_{it}$ for $i = 1, \dots, N$.

5.4 Results and validation

The experimental variograms are calculated using a lag of 14 km along the directions E-W, N-S, NE-SW and NW-SE, with an angle tolerance of 22.5° so as to give complete coverage of the field. At each time, the directional variograms are isotropic and can be grouped into a single omnidirectional variogram. Generally, at each time interval t , the choice of the variogram model requires to fix a set of theoretical functions: a nugget effect, a spherical, an exponential or a gaussian model with different sill and ranges.

A spherical model with varying sill plus a nugget term revealed suitable for all time slices. After some preliminary testing a large neighborhood has been chosen so to ensure that as many samples as possible would be involved in the estimation procedure. In Figure 13 and 14 kriging results at 5:30 am are report. Notice that the number of modelling sites varies with time as it is not always raining everywhere in the area.

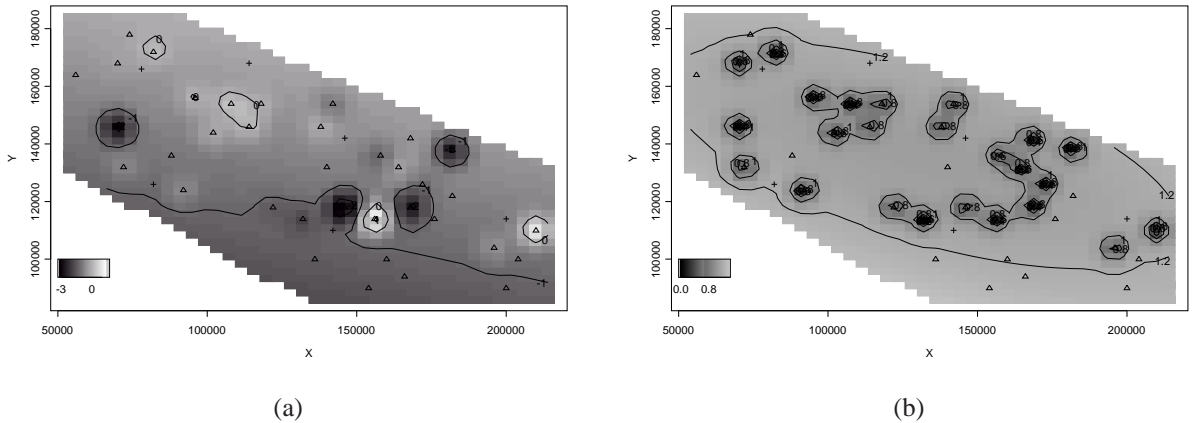


Figure 13: Kriging prediction surface (a) and standard deviation (b) at 5:30 am of state parameter α

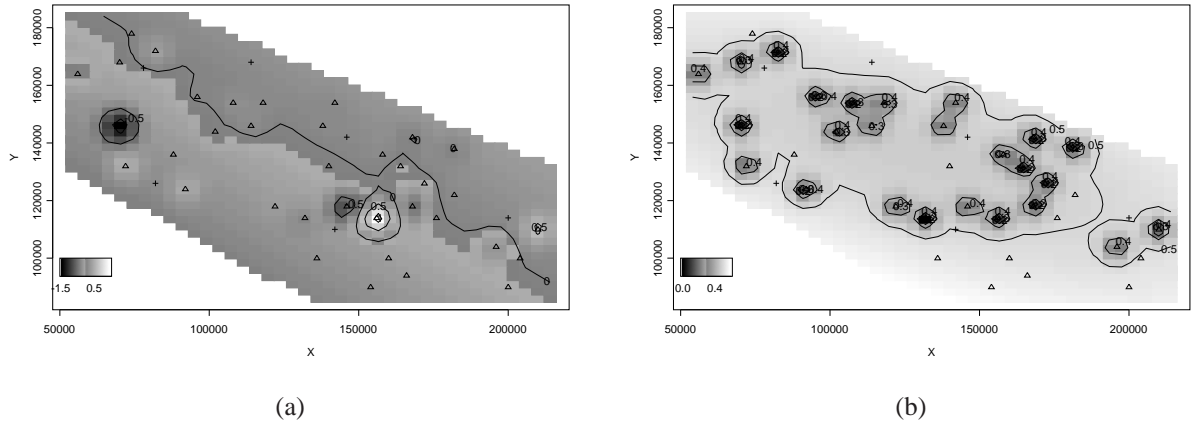


Figure 14: Kriging prediction surface (a) and standard deviation (b) at 5:30 am of state parameter β

The kriging estimates of $\hat{\alpha}_{it}$ and $\hat{\beta}_{it}$, were used to obtain the prediction values \hat{y}_{it} as shown in (6).

Figure 15 shows time series plot of the true rainfall, the estimated raingauge measurements and an empirical confidence interval obtained adding and subtracting two times the standard error. It is important to stress that in order to obtain the estimated rain on the original scale we used the following equation:

$$\hat{R}_{gt} = \exp\{(\hat{\beta}_{it} + \sigma_{\beta}^2/2) * W_{it} + (\hat{\alpha}_{it} + \sigma_{\alpha}^2/2)\} \quad (7)$$

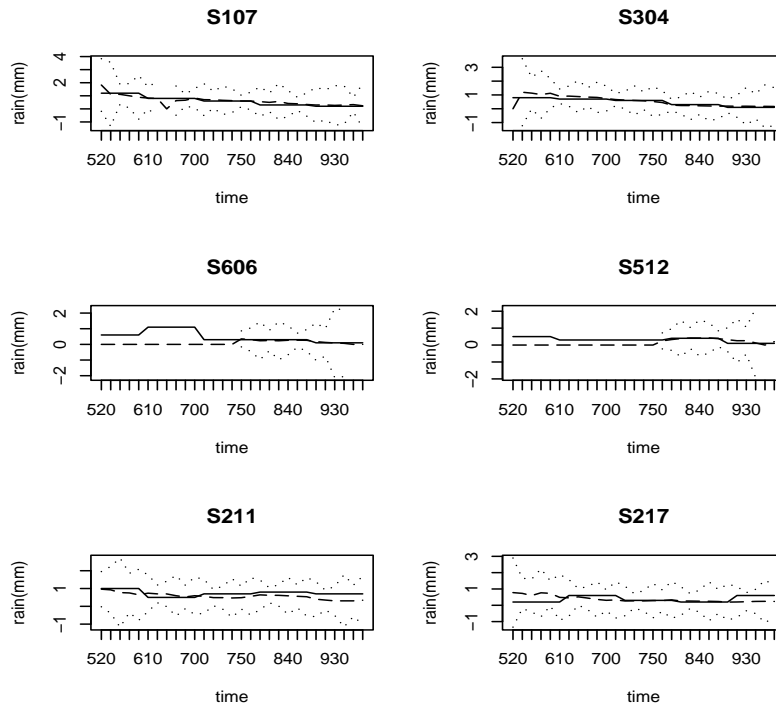


Figure 15: Validation raingauges for the state-space model: True raingauge-rainfall (continous line), estimated rainfall (dashed line) and 2σ empirical confidence interval (dotted)

Predictions follow the pattern of the true rainfall in a better way for sites S107, S304 and S211. The calibrations are worse at other sites, and a general overestimation of the rainfall amount is evident. Furthermore empirical confidence bounds are quite large, often including the zero rain value. Another drawback of this approach is that because of the log transformation of the data only strictly positive radar values are involved in the estimation procedure, then only part of the available information can be used. The empirical mean square error are calculated at each of the six validation sites, and reported in Tab. 7.1. The MSE values are lower at sites S107, S211, S304 and S512.

In order to verify the adequacy of the entertained model, we report a histogram and a Normal Q-Q plot of the standardized residuals calculated at the six validation sites in Figure 16.

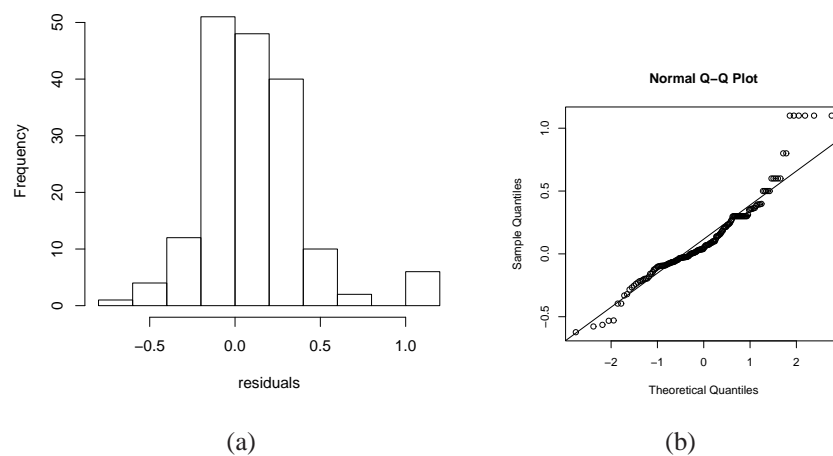


Figure 16: Histogram and Q-Q normal plot of standardized residuals of the six validation sites

From Figure 16(a) we can see that the residuals distribution is quite symmetric with few outliers in the right tail, this behavior is reflected in the normal QQ-plot (Figure16(b)). A plot of residuals versus fitted values, reported in Figure 17, reveals a strong relationship between the fitted values and the residuals most likely due to the discrete nature of radar measurements and the presence of some outliers.

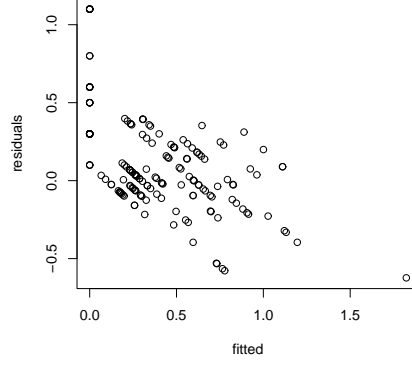


Figure 17: Plot of residuals versus predicted values

This fact suggests that the model to describe the relationship between raingauge rainfall and radar-based rainfall estimation has to be improved. An alternative approach is proposed in the next section.

6 Kriging with External drift

Standard universal kriging assumes that the spatial field under study is the sum of a stationary random function and a polynomial drift:

$$Z(x) = Y(x) + \sum_l a_l f_l(x)$$

in which a_l are deterministic unknown coefficients and f_l are monomials. Under this model, the expectation at location x is given by the following expression:

$$E[Z(x)] = \sum_l a_l f_l(x).$$

The predictor $Z^*(x)$, based on data $z(x_1), \dots, z(x_n)$, is obtained by minimizing the error variance $Var(Z(x) - Z(x)^*)$ under the constraint of unbiasedness $E[Z(x) - Z(x)^*] = 0$ whatever the unknown drift coefficients a_l . This is ensured if the universality conditions $\sum_i \lambda_i f_l(x_i) = f_l(x)$ are satisfied by the linear predictor $Z(x)^* = \sum \lambda_i Z(x_i)$ with weights λ_i . The drift function is usually assumed general and flexible while keeping parameters number small, however better choices are possible if the spatial patterns can be predicted to some extent before the data are available. In some situation it may be of interest to use arbitrary drift functions which results in a particular formulation of universal kriging.

Under an Irf-k model (intrinsic random function of order k), the underlying model is somewhat different and

$$Z(x) = Z_k(x) + m_k(x) \quad (8)$$

consisting of a deterministic part $m_k(x)$, representing the drift as a k-th order polynomial, and a random part $Z_k(x)$ with an associated generalized covariance $K(h)$, where h is the distance

between two locations. The polynomial of order k is a linear combination of functions $f_l(x)$ of the coordinates with coefficients a_l

$$m_k(x) = \sum_{l=0}^L a_l f_l(x) \quad (9)$$

When there are two type of data sets, one containing few samples of good quality but which do not cover regularly the entire field of interest (the random function $Z(x)$), and one containing a large amount of samples covering the whole domain but with poor accuracy (a regionalized variable $s(x)$ considered as deterministic), a well-known method consists in merging the two sources of information using $s(x)$ as an external drift function for the estimation of $Z(x)$. The external drift method consists in integrating into kriging systems supplementary universality conditions about the external drift variable $s(x)$. The function $s(x)$ is known at all locations x_i of the sample as well as at the nodes of the estimation grid. The condition

$$\sum_{i=1}^n \lambda_i s(x_i) = s(x)$$

is added to the universal kriging system independently on the class of covariance $K(h)$. Actually, a class of generalized covariances can only be defined with respect to translation-invariant basis function $f_l(x)$. A kriging system based on translation-invariant and external drift can be written as:

$$\begin{cases} \sum_{b=1}^n \lambda_b K(x_i - x_b) - \sum_{l=0}^L \mu_l f_l(x_i) - \mu_s s(x_i) = K(x_i - x) & \text{for } i = 1, \dots, n \\ \sum_{b=1}^n \lambda_b f_l(x_b) = f_l(x) & \text{for } l = 0, \dots, L \\ \sum_{b=1}^n \lambda_b s(x_b) = s(x) \end{cases} \quad (10)$$

The principle behind this technique is to replace the large scale drift function, usually modeled as a low order polynomial, by a combination of few deterministic functions $f_l(x)$ known over the whole field.

Kriging with the external drift method was successfully applied in climatic studies to map temperature in Scotland (Hudson and Wackernagel (1994)) and for the reconstruction of rainfall fields (Raspa et al. (1997)) moreover it has found application in many fields such as petroleum and gas exploration and hydrogeology.

6.1 Rainfall field reconstruction by kriging with external drift

In this section we apply the kriging with external drift method to the our core dataset. In our study we consider raingauges' data R_g as the $Z(x)$ random function and the radar data R_r , converted to rainfall rate using the Marshall-Palmer relationship, as the external drift function. At this stage, no correlation coefficient between the two variables can be derived, as they are not defined at the same locations. The radar-rainfall background is interpolated at raingauges' sites from the target nodes using a quick bilinear interpolator. A unique neighborhood was chosen because of the small number of samples, no nugget effect was added to perform the estimation. The kriging procedure is applied to each observation time t . The assessment of the predictive performance is tested comparing the predicted rainfall intensity and the true raingauge values at each of the six validation sites and empirical mean square error are computed. The polynomial basic structures (Chiles and Delfiner (1999)) for the determination of the optimal generalized covariance used in the estimation procedure are:

- a linear generalized covariance term $K(h) = -b_0|h| + b_1|h|^3$;
- a spline generalized covariance $K(h) = b_s|h|^2 \log|h|$.

where $|h| = \sqrt{h_1^2 + h_2^2 + \dots + h_n^2}$ and h_i are the distances between sites. For instance, the resulting optimal model used for the estimation, on the first temporal slice (April 11, 1992 at 5:20 a.m), is given by a linear term and a spline term with coefficients 0.166 and 0.012 respectively. Estimation results are visualized in Figure 18. Figure 18(b) shows the map of the estimated standard deviations. Rain estimates at grid nodes keep values ranging from 0 mm to 1.64 mm.

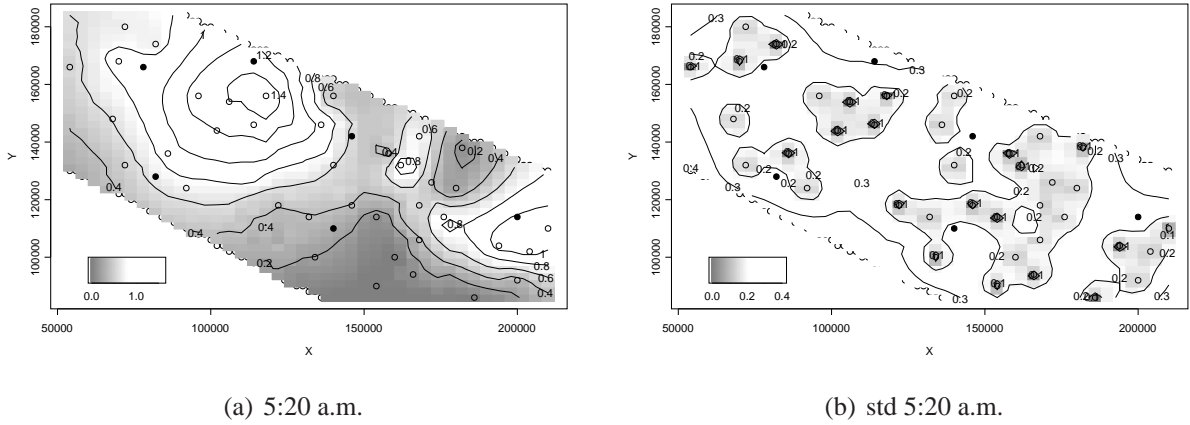


Figure 18: April 11, 1992 at 5:20 a.m.(a):Estimated rainfall as background and raingauges' location; (b): Standard deviation of estimation and raingauges' location.

The map of estimated values shows higher values of estimated rain where raingauges recorded higher rainfall values and decreasing values elsewhere. Standard deviation values are smaller near the raingauges and increase with distance. Maps obtained every 10 minutes show an increase of rainfall rate along the SE direction until 9:00 a.m.; after this time the rainfall rate constantly decreases towards zero. Again, maps of standard deviation, record smaller values near raingauges and higher values far from gauges. In conclusion, is important also to stress the usual drawbacks of this method:

- the final map resembles the drift map as soon as the two variables are highly correlated and tends to ignore the drift map in the opposite case;
- the drift information is used as a deterministic function, and then the estimation error does not take into account the variability of the drift and the uncertainty in the drift measurements;

6.2 Validation

The validation procedure is performed always on the same six raingauges, shown in Figure 1. Figure 19 shows time series plot of the true rainfall, the estimated raingauge measurements and approximate 95% confidence intervals obtained as estimated values plus and minus two times the standard errors. Better estimates are obtained at sites S304 and S606 and their standard errors are generally smaller. In general, the estimated rainfall follows the behavior of the true

rainfall. Furthermore, the true raingauge measurements are within the 95% intervals, as would be expected. However, all six validation gauges are located close to the calibration gauges and we cannot verify if the calibrations are still accurate when the distance from calibration sites increase. Moreover, the standard deviations increase with the distance from the raingauge network. The empirical mean square errors were calculated at each of the six validation sites, and results are shown in Tab.7.1. The MSE values confirm that, at each validation site, the estimates obtained through the KDE method are very similar to the true rainfall.

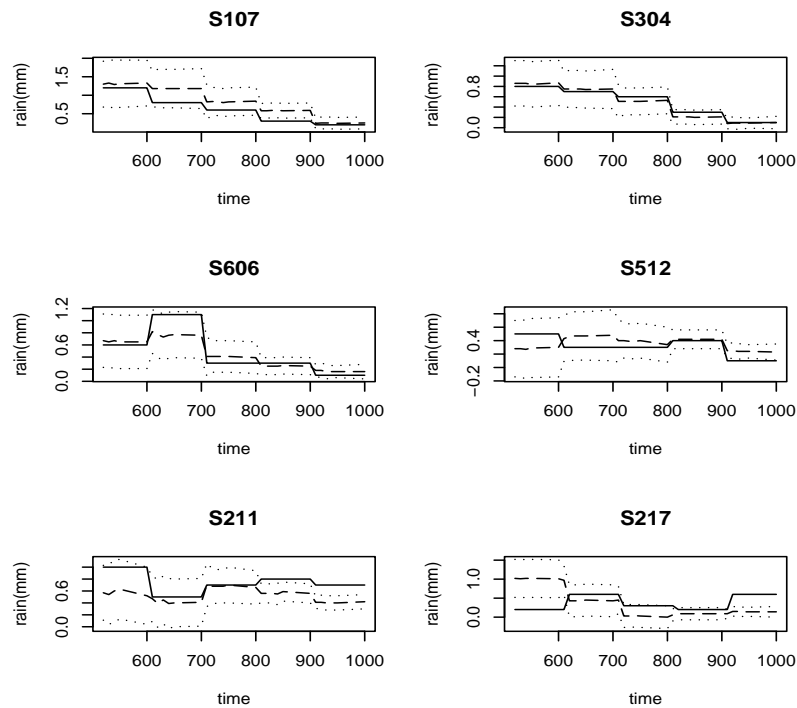


Figure 19: Validation raingauges for the KDE: True raingauge-rainfall (continous line), estimated rainfall (dashed line) and 2σ empirical confidence interval (dotted)

In order to verify the adequacy of the entertained model, we report a histogram and a Normal Q-Q plot of the standardized residuals calculated at the six validation sites (Figure 20).

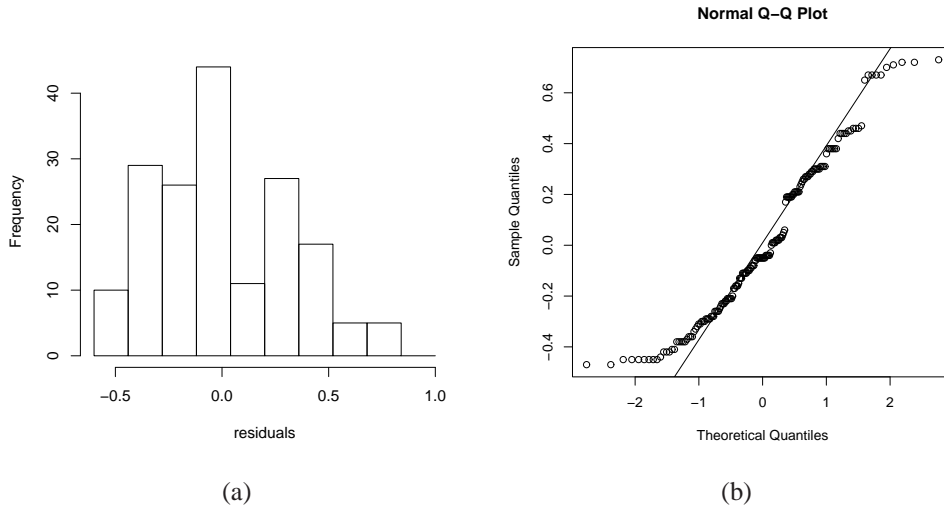


Figure 20: Histogram and Q-Q norm plot of standardized residuals of the six validation sites

The histogram in Figure 20(a) reveals a departure of residuals distribution from the normal distribution which is reflected in the normal QQ-plot (20(b)). The latter shows a curved departure from linearity toward the middle part of the plot. A plot of residuals versus fitted values, reported in Figure 21, reveals again the relationship between the fitted values and the residuals but now this relation is less strong respect to those one obtained by the state-space model.

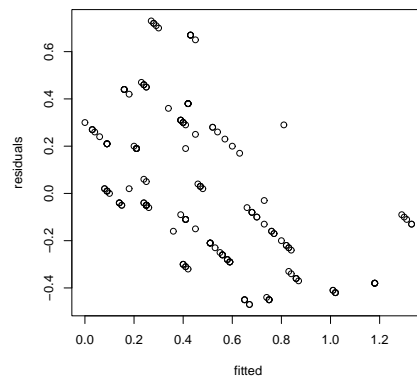


Figure 21: Plot of residuals versus predicted values

7 Comparing results

Results obtained, in terms of MSE, with the proposed approaches are quite different. From Table 7.1 it can be noticed that modelling the rainfall by the Kriging with an external drift returned reductions in the average mean square errors; in three sites they are lower than those obtained through the space-time approach for each validation site. The reason why this happens is proposed below.

A fundamental innovation in this work, with respect to the study previously conducted on the Italian rain enhancement project, was the introduction of calibrated radar data that until now were used only for visual inspection. However, the quality of radar data is extremely poor. The radar-based rainfall estimations are affected by errors that influence the relationship with the true rainfall. This fact strongly affect the model's assumptions for the state space approach while it is less relevant in KDE procedure. The latter because in this case radar data play the role of background map affecting in a smaller measure the estimation procedure.

As a further term of comparison, in Table 7.1 the empirical mean square errors for the proposed approaches and for the Ordinary Kriging (OK) of rainfall alone as measured by the raingauges network are compared. This last technique has been applied using a global neighborhood, a spherical variogram with sill and nugget changing with time and with common range (21000 m). In terms of MSE the KDE method performs better then the other two, moreover by looking at the plots with confidence intervals (Figure 22) we can see that OK estimates are the least reliable. Indeed most of the observed values lies outside the $2\sigma^2$ confidence interval telling us how little reliable these estimates are. On the other hand the KDE method shows a considerably better result in terms of empirical confidence interval (Figure 19).

Validation sites	KDE	State space	OK
S107	0.0597	0.0516	0.0237
S211	0.0629	0.0584	0.089
S217	0.1940	0.0842	0.176
S304	0.0044	0.0458	0.0107
S512	0.0195	0.0820	0.0344
S606	0.0273	0.326	0.0459
Overall Mse	0.0613	0.108	0.0633

Tab 7.1: Comparing MSE of the space-time approach, the KDE method and the Ordinary Kriging of rain

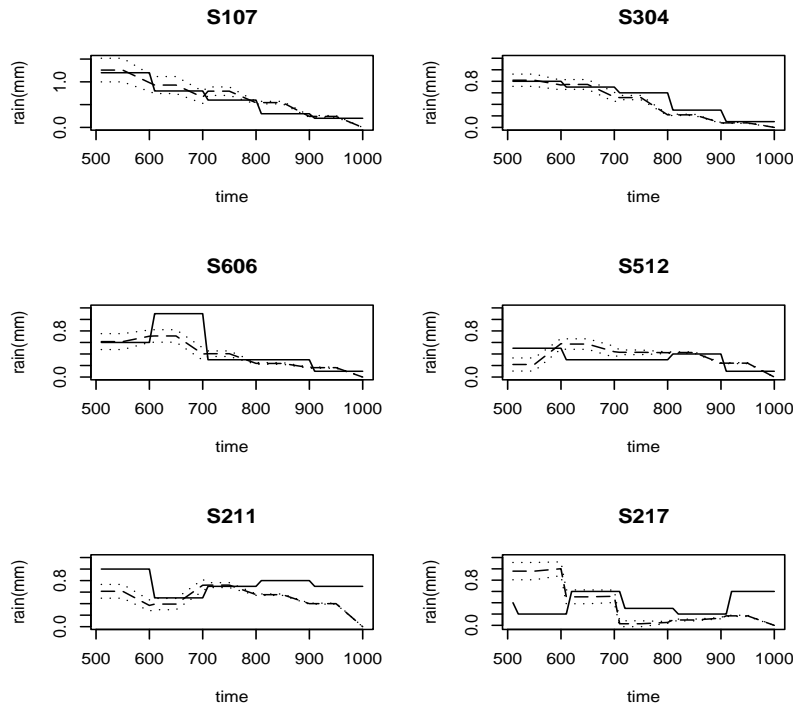


Figure 22: Validation raingauges for the O.K.: True rain gauge-rainfall (continuous line), estimated rainfall (dashed line) and 2σ empirical confidence interval (dotted)

8 Conclusion

The introduction of a C-band digital weather radar, scanning the whole area every five minutes, allowed us to introduce a new element of investigation in the project evaluation task permitting the reconstruction of the rainfall field over an area larger than the one covered by the rain gauge network. However, rainfall and radar measurements are notably different: on one hand the first ones give a direct measure, spatially punctual and time integrated, of ground rainfall; on the other hand, the second ones give an indirect measure of precipitation, on the air, and integrated in space and at a given point in time. The well-known Z-R relationship suggests the type of link existing between the two measurements, however it is not an exact equation and its use may not be always correct when the aim is to build a model able to provide estimates of rainfall intensity over a region larger than the one covered by the ground rain gauge network. The Marshall-Palmer relationship provided a first approximation to the rainfall rates throughout the radar field and several types of calibration of the estimated values were tested and compared. The first one proposed, using the calibration factor, i.e. the ratio between rainfall as measured at ground level and rainfall measured by radar, led to a general reduction in the errors in radar-derived rainfall estimates, however large spatial errors still remain. The second proposed strategy reflects the fact that the ground data are spatially sparse, but temporally dense. The model implies the fitting of a linear state-space time series model at each site. In the multi-site model, Kriging surface of the state variables, associated with the n sites at which ground measurements are available, were obtained through Ordinary Kriging for each time-interval. This, in turn, led to prediction of ground rainfall intensity at arbitrary locations, for which only radar data exist. In the fitting procedure we left out six sites reserved for validation purposes. Anal-

ysis showed relatively small MSE values for these six sites and approximate predictions and a further method was proposed and compared.

The use of the Kriging with external drift allowed us to obtain at each time-interval, maps of rainfall data using the radar data as an external drift to add to the kriging equations. The integration of radar maps improved the estimating accuracy, as showed by the smaller MSE values at the six validation sites and also has the advantage of being computationally efficient. However, kriging type estimates are highly reliable only inside the domain in which ground measurements are taken. As we are interested in evaluating extra-area effects we need a further strategy to improve our estimates. Moreover, we still need to build an integrated space-time model which is consistent with the data and which captures the essential features of the observed pattern of spatial and temporal joined dependence. A new study is currently applying the model proposed by Sahu and Mardia (2005) that implies the use of drift functions in space and of correlations (first order Markov structure) in time in a full Bayesian framework.

Acknowledgements We would like to thank prof. K. Mardia, dr. C. Goodall and prof. P.L.Conti for the useful discussions and encouragement. The UCEA staff for the many technical explanations. A special thank goes to prof. C. Gaetan for giving us the first useful hint.

References

- Austin, P. (1987). Relation between measured radar reflectivity and surface rainfall. *Mon. Wea. Rev.* 115, 1053–1070.
- Brown, P., P. Diggle, M. Lord, and P. Young (2001). Space-time calibration of radar-rainfall data. *Journal of the Royal Statistical Society, Series C* 50(2), 221–241.
- Chiles, J. and P. Delfiner (1999). *Geostatistics, Modelling Spatial uncertainty*. Wiley, New York.
- Ciach, J. and W. Krajewski (1999). Radar-raingauge comparison under observational uncertainties. *J. Appl. Meteor.* 38, 1519–1525.
- Collinge, V. and P. Young (1993). *Weather radar calibration: Systems Approach* (Oxford; Pergamon ed.), pp. 706–710. Concise Encyclopedia of Environmental Systems. ed. P.C. Young.
- Doviak, R. and S. Zrnic (1984). *Doppler Radar and Weather Observations*. Academic Press, Inc.
- Dunn, P. (2003). Precipitation occurrence and amount can be modelled simultaneously. *Working Paper, Series SC-MC-0305, Faculty of Sciences, USQ*.
- Gagin, A. (1981). The israeli rain enhancement experiments. a physical overview. *J. Wea. Modif.* 13, 1–13.
- Hudson, G. and H. Wackernagel (1994). Mapping temperature using kriging with external drift: theory and an example from scotland. *International Journal of Climatology* 14, 77–91.

- Krajewski, W. (1987). Cokriging radar-rainfall and rain gage data. *Journal of Geophysical Research* 92(D8), 9571–9580.
- Krajewski, W. (1997). Rainfall estimation using weather radar and ground stations.
- Legates, D. (2000). Real-time calibration of radar precipitation estimates. *Professional Geographer* 52, 235–246.
- Marshall, J. and W. Palmer (1948). The distribution of raindrops with size. *J. Meteor.* 5, 69–76.
- Matsoukas, C., S. Islam, and R. Kothari (1999). Fusion of radar and raingauge measurements for an accurate estimation of rainfall. *J. of Geophysics Res.* 104, 31437–31450.
- Orasi, A. (2004). *Reconstruction of rainfall fields by spatio-temporal models for the analysis of a rain enhancement experiment in Southern Italy*. Ph. D. thesis, University of Bologna.
- Orasi, A. and G. Jona-Lasinio (2004). Statistical aspects of rainfall fields in southern italy during a rain enhancement experiment. Submitted.
- Raspa, G., M. Tucci, and R. Bruno (1997). *Reconstruction of rainfall fields by combining ground raingauges data with radar maps using external drift method* (Kluwer Academic Publishers ed.), Volume 2 of *Geostatistics Wollongong '96*, pp. 1306–1315. E.Y. Baafi and N.A. Schofield eds.
- Rodriguez-Iturbe, I., D. Cox, and V. Isham (1987). Some models for rainfall based on stochastic point processes. *Proceedings of the Royal Society of London Series A* 410, 269–288.
- Rodriguez-Iturbe, I., D. Cox, and V. Isham (1988). A point process model for rainfall: further developments. *Proceedings of the Royal Society of London Series A* 417, 283–298.
- Sahu, S. and K. Mardia (2005). A bayesian kriged-kalman model for short-term forecasting of spatio-temporal processes. *Journal of the Royal Statistical Society, Series C* 54(1), 223–244.
- Sansó, B. and L. Guenni (1999). Venezuelan rainfall data analysed using a bayesian space-time model. *Applied Statistics* 48, 345–362.
- Sansó, B. and L. Guenni (2000). A non-stationary multi-site model for rainfall. *JASA* 95, 1189–1200.
- Seo, D., W. Krajewski, and D. Bowles (1990). Stochastic interpolation of rainfall data from raingages and radar using cokriging. 1. design of experiments. *Water Resour. Res.* 26, 469–477.
- Seo, D., W. Krajewski, D. Bowles, and A. Azimi-Zonooz (1990). Stochastic interpolation of rainfall data from raingages and radar using cokriging. 2. results. *Water Resour. Res.* 26, 915–924.
- Smith, R. (1994). *Spatial modelling of rainfall data* (Wiley, New York ed.), pp. 19–42. *Statistics for the environment 2: Water Related Issues*. eds. Barnet, V. Feridum Turkman, K.
- Stern, R. and R. Coe (1984). A model fitting analysis of rainfall data. *Journal of the Royal Statistical Society, Series A* 147, 1–34.
- W.M.O. (2001). Statement on weather modification.

Wood, S., D. Jones, and R. Moore (2000). Static and dynamic calibration of radar data for hydrological use. *Hydrology and Earth System Sciences* 4(4), 545–554.

Zawadzki, I. (1975). On radar-raingauge comparison. *J. Appl. Meteor.* 14, 1430–1436.

Zawadzki, I. (1984). Factors affecting the precision of radar measurements of rain. *Preprints, 22nd Radar Meteorology Conf., Zurich (American Meteorological Society)*, 251–256.